

Short Timescale Correlations Between Line and Continuum Fluxes in Cygnus X-1

Thomas J. Maccarone

Scuola Internazionale Superiore di Studi Avanzati, via Beirut, n. 2-4, Trieste, Italy, 34014

Paolo S. Coppi

Department of Astronomy, Yale University, P.O. Box 208101, New Haven CT USA 06520-8101

ABSTRACT

We present the results of 16-s time scale spectral fits for Cygnus X-1 in the soft state and in the transition state, using a Comptonised blackbody plus an iron line. On these timescales, we find that the continuum source flux can vary by factors 2-3 and that the iron line intensity appears to track these changes well, i.e., the inferred equivalent width of the line remains constant to within the errors. We also find no significant changes in the seed (blackbody) photon temperature, while the properties of the Comptonising corona clearly do vary, with the spectral hardness and flux generally being correlated. The corona therefore seems to be the overall driver for the rapid timescale variability observed in the soft and transition states. These results are consistent with the Fourier resolved spectroscopy results of Gilfanov et al. (2000) that indicate the iron line shows rapid flux variations while the blackbody component does not and suggest that the iron line flux in fact tracks continuum changes down to very short timescales. We extend this work by showing that not only the variability amplitudes, but also the *phases* of the iron line and continuum components are identical. We note that the short timescale variability properties of the soft and transition states are actually not very different from those of the hard state, suggesting that the corona is the main cause of rapid variability in that state too, and hence that the mechanism responsible for the corona is similar in all three states.

Key words: accretion, accretion discs – X-rays: binaries – X-rays: individual: Cygnus X-1

1 INTRODUCTION

The spectra of accreting black holes in the soft state generally consist of a strong quasi-thermal component, generally assumed to come from a cold accretion disc (Shakura & Sunyaev, 1973), a power law tail thought to originate in a corona of hot electrons above the disc, and some additional features (a Compton reflection bump and some iron emission lines) thought to result from reprocessing of the hard photons from the corona by the disc (Basko, Sunyaev, & Titarchuk 1974; George & Fabian 1991).

Several studies of active galactic nuclei (AGNs) have shown that changes in the profile and equivalent width of the iron line can be related to continuum changes (Iwasawa et al. 1996; Yaqoob et al. 1996; Nandra et al. 1999; Wang et al. 1999; Weaver, Gelbord, & Yaqoob 2000), suggesting that the iron line is indeed due to reprocessing of the continuum by ambient cold matter, e.g., the accretion disc. The results of the AGN studies, however, have been somewhat

ambiguous and are likely complicated by factors that are less likely to arise in compact binary systems. Reprocessing from a dusty torus (Antonucci & Miller 1985) and the possibility that the iron line does not come exclusively from the disc are two such factors (Weaver & Reynolds 1998). Studies of binaries thus should prove useful in providing confirmation that the iron lines from accreting black holes really do represent reprocessing of coronal X-rays by the disc and in disentangling the disc components' contributions from other contributions.

Timing characteristics have been used to provide evidence for the applicability of reflection models in the canonical Galactic black hole candidate Cygnus X-1 through the technique of Fourier resolved spectroscopy (Gilfanov, Churazov, & Revnivtsev, 2000). This technique works by Fourier transforming the lightcurve of Cyg X-1 in several energy bands, then re-assembling a spectral energy distribution at each Fourier frequency to determine the spectrum of the component of the lightcurve that varies on a particular

timescale. Their analysis found that the reflected component and the primary emission tracked each other down to timescale less than about 30 ms. It also showed that the iron line flux is roughly constant for frequencies ≥ 30 Hz, giving an estimate for the inner disc size.

A significant drawback of this technique, however, is that it loses phase information. The iron line features cannot be definitively shown to be due to reflection unless some correlation is found between the phase of the iron line and the phase of the incident hard photons. This paper seeks to complement the Fourier resolved spectrum by working instead in the time domain. While photon statistics do not permit us to probe down to the very shortest timescales, we nonetheless can obtain useful spectral information down to short timescales ~ 10 seconds, where significant continuum flux variability is present. By direct spectral fitting, we demonstrate that the iron line equivalent width remains constant on short timescales in both the soft state and the transition state of Cygnus X-1, i.e., that the iron line tracks continuum changes. At the same time, under the assumption that the observed continuum is Comptonised radiation, we find no evidence for significant changes in the seed photon distribution. This suggests that the mechanism responsible for powering the hot coronal electrons is responsible for most of the observed flux variations, and that the disc is relatively quiescent. In section 2 below, we outline our data reduction procedure. In section 3 we discuss the fitting procedure and the model used. In section 4, we show fits both for the 16 second timescales we emphasize in this work, and for the full RXTE dwells on the source in order to assess the problems that may be induced by fitting on the shorter timescales with the lower signal to noise. In section 5, we compare short timescale variability in the soft and transition states to that in the hard state and show that it is likely that coronal changes drive the variability in all three states. In section 6, we summarize all our conclusions.

2 OBSERVATIONS

Analysis is presented of eight RXTE (Bradt, Rothschild, & Swank, 1993) observations taken while Cygnus X-1 was in its “soft state” in June of 1996 (proposal 10512). The soft state of Cygnus X-1 shows a stronger power law spectral tail and more variability than typical black hole binary soft states and may actually be an intermediate state (see Nowak 1995 for a review of spectral state nomenclature). The data are prepared using the standard RXTE screening criteria: earth elevation greater than 10 degrees, offset less than 0.01 degrees, all five proportional counter units on, and appropriate time separation both before and after South Atlantic Anomaly Passages. Spectra are then extracted on a 16-second time scale to allow for background subtraction and response matrices are computed all using the standard FTOOLS 5.0.4 routines. All layers and all 5 Proportional Counter Units are included, since the source dominates the background and the most possible source counts are desired. Response matrices are computed using PCARMF version 7.10. The total duration of the data analyzed is 9856 seconds (9546 seconds of live time). The 16-second time scale is chosen because it is convenient for background subtraction

purposes and because counting statistics do not permit studies on much shorter time scales.

Results are also shown from the transition state into and out of the soft state (RXTE proposal 10412). These observations were taken in May and August of 1996, respectively. The same selection criteria specified above are used to determine the good time intervals. The total duration of the transition state data analyzed is 14096 seconds (13354 seconds of live time). Finally, the hard state data from December of 1997 (RXTE proposal 30158) were also analyzed, but the low count rates do not allow for strong constraints to be placed on the variations of the equivalent widths of the iron lines in this state.

3 ANALYSIS

3.1 Discussion of Systematic Errors

Observations of iron lines are not straightforward with an instrument like RXTE that has poor energy resolution. Iron line variability has been seen in previous RXTE observations (e.g. Lee et al 2000), but care must be taken with the data analysis to avoid spurious results. In order to justify our choice of energy channels and to present evidence that the correlations to be discussed are real and not instrumental artefacts, we present spectral fits to the two Crab observations taken most nearly in time to the Cyg X-1 observations presented here. In both cases, the neutral hydrogen column is fixed to the Galactic value, $3.8 \times 10^{21} \text{ cm}^{-2}$. The power law index of the Crab is fit to be 2.175. We then fit the normalisation both with all channels included and with just the channels from 3.5-10 keV included. For the Crab spectrum just after our observations (July 23, 1996), the deviations are less than 1% in the 3.5-10 keV range and generally less than 0.5% when only the channels from 3.5-10 keV are used for fitting the normalisation. The residuals are slightly larger for the observation taken before Cyg X-1 had begun its transition to the high state (May 3, 1996). The normalisations of the two fits were consistent within much less than 1%. Since the accuracy of the response matrix is significantly worse below 3.5 keV, we ignore these channels. We plot the results of the July 23 fit in Figure 5.1. The χ^2/ν values for the two fits are 5.8 and 2.9 for the May 3 and July 23 fits respectively (with 17 bins and hence 15 degrees of freedom for each). While these are formally quite bad fits, the statistical errors for even a few hundred seconds of observation of a source as bright as the Crab are quite small, and the systematic errors dominate. To estimate the appropriate systematic errors, we add systematic errors to all channels and re-fit the data until a χ^2/ν of 1.0 is achieved. We find that a 0.35% error is required for the May 3 observation and an 0.3 % error is required for the July 23 observation. While this estimate of the systematic errors is not strictly correct (as the systematic errors in the different channels could be correlated), it represents the best estimate that can be made with the given data.

3.2 Spectral fits

Using XSPEC 10.0 (Arnaud 1996), the spectra are fit from 3.5 keV to 10 keV (including 17 channels) with a simple

ObsID	Start Time	Stop Time
10412-01-02-00	22/05/96 17:58:10	22/05/96 19:49:13
10412-01-01-00	23/05/96 14:29:04	23/05/96 18:08:13
10412-01-03-00	30/05/96 07:57:58	30/05/96 08:45:13
10512-01-07-00	16/06/96 00:07:30	16/06/96 00:41:13
10512-01-07-02	16/06/96 04:55:31	16/06/96 05:44:13
10512-01-08-01	17/06/96 01:44:32	17/06/96 02:24:13
10512-01-08-02	17/06/96 04:56:32	17/06/96 05:44:13
10512-01-08-00	17/06/96 08:08:32	17/06/96 09:08:13
10512-01-09-02	18/06/96 03:21:34	18/06/96 04:04:13
10512-01-09-00	18/06/96 06:34:33	18/06/96 07:26:13
10512-01-09-01	18/06/96 09:46:33	18/06/96 10:46:13
10412-01-05-00	11/08/96 07:21:46	11/08/96 08:25:13
10412-01-06-00	11/08/96 15:25:58	11/08/96 15:52:13

Table 1. The data analyzed for this work. Dates are presented in DD/MM/YY format. The observations from proposal 10512 are the soft state observations while those from proposal 10412 are the transition state observations. The hard state data analyzed are all the pointings from RXTE proposal 30158.

model consisting of a comptonised blackbody component (compbb in XSPEC - Nishimura, Mitsuda, & Itoh, 1986), a Gaussian component to fit the iron line. The spectral resolution of RXTE is not sufficient to provide strong constraints on the shape of the feature we call an iron line, so other explanations for this flux remain possible. Still, it is the most physically likely explanation for this excess flux, so we refer to this feature as an iron line throughout the remainder of the paper. This model was multiplied by photoelectric absorption (wabs). When more complicated models were fit to the data (such as pexrav - Magdziarz & Zdziarski 1995 to replace the power law component), the increased number of free parameters resulted in degenerate fits and the individual parameters had substantially larger error bars. By ignoring the channels above 10 keV, we are able to exclude the range of energies where reflection is likely to be an important contributor to the broad continuum features in the spectrum. While using complicated models over a larger range of energies might, in principle, allow us to constrain the distribution of the Comptonising electrons in the corona and the reflection fraction (as in Frontera et al. 2000), such models are too computationally intensive for applications to our short timescale data, and the lever arm from hard photons needed to constrain the parameters of such models suffers from poor statistics on short timescales. The iron line center is constrained to lie between 6.2 and 7.0 keV (but always fits best to energies between 6.4 and 6.5 keV), the neutral hydrogen column density is fixed at $5 \times 10^{21} \text{ cm}^{-2}$, according to ASCA results (see e.g., Gierlinski et al. 1999). All the other parameters were allowed to float freely. A systematic error of 0.3% is included as suggested by the Crab fits. We also plot the results of a ratio of the source data to the Crab data in Figure 5.1b, and of a 16 second integration in Figure 5.1c.

In Table 2 we present the results of spectral fits to the full observations shown here, with an iron line included. Since there are 17 energy channels, one can fit the 7 parameter model with 10 degrees of freedom. We also tabulate the $\Delta\chi^2$ that results from removing the iron line from the model. Fits of a reflection model (i.e. pexriv) with no Gaussian component are similarly bad.

A more phenomenological model (disc blackbody + power law + Gaussian) gives an acceptable fit in terms of χ^2/ν , but results in an artificially low line energy (~ 6.2

keV) and an artificially high line equivalent width ($> 1 \text{ keV}$). This problem is relatively severe because the two continuum components intersect near 6 keV. The real continuum of a Comptonised spectrum shows strong curvature at energies where the seed blackbody spectrum begins to fall sharply, and the phenomenological model fails to reproduce that curvature. The Gaussian component drifts to lower energy and to higher flux level to fill in the missing flux from the incorrect estimation of the continuum. If the flux at the lowest energies contains a significant contribution from Comptonised radiation, as suggested by the more detailed long-timescale fits of Gierlinski et al. (1999) and Frontera et al (2000), then the temperature of the soft component is also systematically overestimated by phenomenological model, as the peak energy in the spectrum is shifted upwards by the Comptonisation process driving the best fit temperature to larger values as well. Using a Comptonised blackbody as the continuum model is not computationally expensive and avoids all these problems. As we shall see, doing so also gives parameters in reasonable agreement with those obtained using the more detailed, wider energy range fits.

4 RESULTS

4.1 Transition state - full integrations

In the transition state, the blackbody temperature is always fit by a value consistent with 400 eV. The value of the disc temperature as well as the values of all the line parameters (line energy, physical width and equivalent width) are consistent with those found from joint fits to ASCA/RXTE observations taken during the same transition state (Frontera et al., 2001) within the 90% error bars, which lends confidence to the interpretation that the continuum is well modeled by compbb in the energy range examined and that the response of RXTE is sufficient for making these measurements (since the ASCA observations will place much stronger constraints on the parameters of line features than RXTE does). The iron line equivalent width seems to rise going into the soft state, as the two lowest equivalent width observations were taken during the earliest part of the transition state, but the equivalent widths of the line in the different transition state observations are all consistent with one another at the 90% confidence level, so no strong claims can be made.

ObsID	BB Temp	KT_{cor}	τ	LE	LW	LN	χ^2/ν	$\Delta\chi^2$	EqW	Flux
10412-01-01-00	$0.43 \pm_{-0.10}^{+0.12}$	$21.1 \pm_{-1.8}^{+5.5}$	$1.53 \pm_{-0.77}^{+0.16}$	$6.46 \pm_{-0.10}^{+0.05}$	$0.71 \pm_{-0.06}^{+0.14}$	$4.4 \pm_{-0.4}^{+1.8} \times 10^{-2}$	0.30	2600	230	14
10412-01-02-00	$0.37 \pm_{-0.06}^{+0.11}$	$25.1 \pm_{-0.9}^{+0.8}$	$0.83 \pm_{-0.10}^{+0.06}$	$6.46 \pm_{-0.06}^{+0.03}$	$0.66 \pm_{-0.05}^{+0.07}$	$4.2 \pm_{-0.3}^{+0.6} \times 10^{-2}$	0.23	1700	242	13
10412-01-03-00	$0.38 \pm_{-0.10}^{+0.12}$	$26.1 \pm_{-1.6}^{+3.0}$	$0.73 \pm_{-0.46}^{+0.14}$	$6.47 \pm_{-0.05}^{+0.06}$	$0.70 \pm_{-0.06}^{+0.07}$	$4.5 \pm_{-0.4}^{+0.5} \times 10^{-2}$	0.55	2300	269	9.0
10412-01-05-00	$0.42 \pm_{-0.10}^{+0.11}$	$21.8 \pm_{-1.5}^{+1.6}$	$1.24 \pm_{-0.06}^{+0.12}$	$6.43 \pm_{-0.07}^{+0.06}$	$0.73 \pm_{-0.09}^{+0.09}$	$4.9 \pm_{-0.5}^{+0.8} \times 10^{-2}$	0.46	2200	275	14
10412-01-06-00	$0.41 \pm_{-0.08}^{+0.11}$	$22.6 \pm_{-1.3}^{+1.4}$	$1.03 \pm_{-0.11}^{+0.13}$	$6.38 \pm_{-0.09}^{+0.07}$	$0.75 \pm_{-0.08}^{+0.09}$	$5.9 \pm_{-0.7}^{+1.0} \times 10^{-2}$	0.16	1900	261	17
10512-01-07-00	$0.38 \pm_{-0.09}^{+0.08}$	$26.1 \pm_{-1.1}^{+2.5}$	$0.61 \pm_{-0.15}^{+0.10}$	$6.41 \pm_{-0.08}^{+0.04}$	$0.74 \pm_{-0.08}^{+0.09}$	$5.0 \pm_{-0.9}^{+2.7} \times 10^{-2}$	0.47	2050	361	11
10512-01-07-02	$0.37 \pm_{-0.05}^{+0.07}$	$26.7 \pm_{-0.9}^{+0.6}$	$0.51 \pm_{-0.15}^{+0.07}$	$6.41 \pm_{-0.09}^{+0.05}$	$0.75 \pm_{-0.08}^{+0.09}$	$3.8 \pm_{-0.7}^{+2.0} \times 10^{-2}$	0.52	2150	365	9.0
10512-01-08-00	$0.38 \pm_{-0.09}^{+0.08}$	$26.1 \pm_{-1.1}^{+2.5}$	$0.61 \pm_{-0.15}^{+0.10}$	$6.41 \pm_{-0.08}^{+0.04}$	$0.74 \pm_{-0.08}^{+0.09}$	$5.0 \pm_{-0.9}^{+2.7} \times 10^{-2}$	0.47	2700	344	15
10512-01-08-01	$0.37 \pm_{-0.08}^{+0.09}$	$27.9 \pm_{-3.0}^{+3.5}$	$0.46 \pm_{-0.16}^{+0.10}$	$6.37 \pm_{-0.10}^{+0.08}$	$0.77 \pm_{-0.10}^{+0.08}$	$2.9 \pm_{-0.7}^{+2.5} \times 10^{-2}$	0.51	1200	369	6.5
10512-01-08-02	$0.38 \pm_{-0.09}^{+0.08}$	$26.1 \pm_{-1.1}^{+1.0}$	$0.61 \pm_{-0.15}^{+0.10}$	$6.41 \pm_{-0.08}^{+0.04}$	$0.74 \pm_{-0.08}^{+0.09}$	$5.0 \pm_{-0.9}^{+2.7} \times 10^{-2}$	0.47	2550	398	10
10512-01-09-00	$0.35 \pm_{-0.06}^{+0.05}$	$28.0 \pm_{-0.7}^{+1.5}$	$0.37 \pm_{-0.11}^{+0.08}$	$6.49 \pm_{-0.12}^{+0.06}$	$0.73 \pm_{-0.07}^{+0.07}$	$2.3 \pm_{-0.3}^{+0.6} \times 10^{-2}$	0.35	2200	356	5.8
10512-01-09-01	$0.38 \pm_{-0.09}^{+0.08}$	$26.1 \pm_{-1.1}^{+2.5}$	$0.61 \pm_{-0.15}^{+0.10}$	$6.41 \pm_{-0.08}^{+0.04}$	$0.74 \pm_{-0.08}^{+0.09}$	$5.0 \pm_{-0.9}^{+2.7} \times 10^{-2}$	0.27	3150	367	13
10512-01-09-02	$0.38 \pm_{-0.09}^{+0.08}$	$26.1 \pm_{-1.1}^{+2.5}$	$0.61 \pm_{-0.15}^{+0.10}$	$6.41 \pm_{-0.08}^{+0.04}$	$0.74 \pm_{-0.08}^{+0.09}$	$5.0 \pm_{-0.9}^{+2.7} \times 10^{-2}$	0.87	1600	411	5.7

Table 2. The best fit parameters (along with their 90% error intervals) for the full integrated observations of Cygnus X-1. The column names are, in order, Observation ID number, comptonised blackbody temperature in keV, temperature of the corona in keV, the optical depth of the corona, line energy, line width, line normalization in XSPEC units, χ^2/ν for the best fits, $\Delta\chi^2$ when the iron line is removed, the equivalent width of the best fit iron line in eV, and the integrated flux from 3.5 to 10 keV in 10^{-9} ergs/cm²/sec.

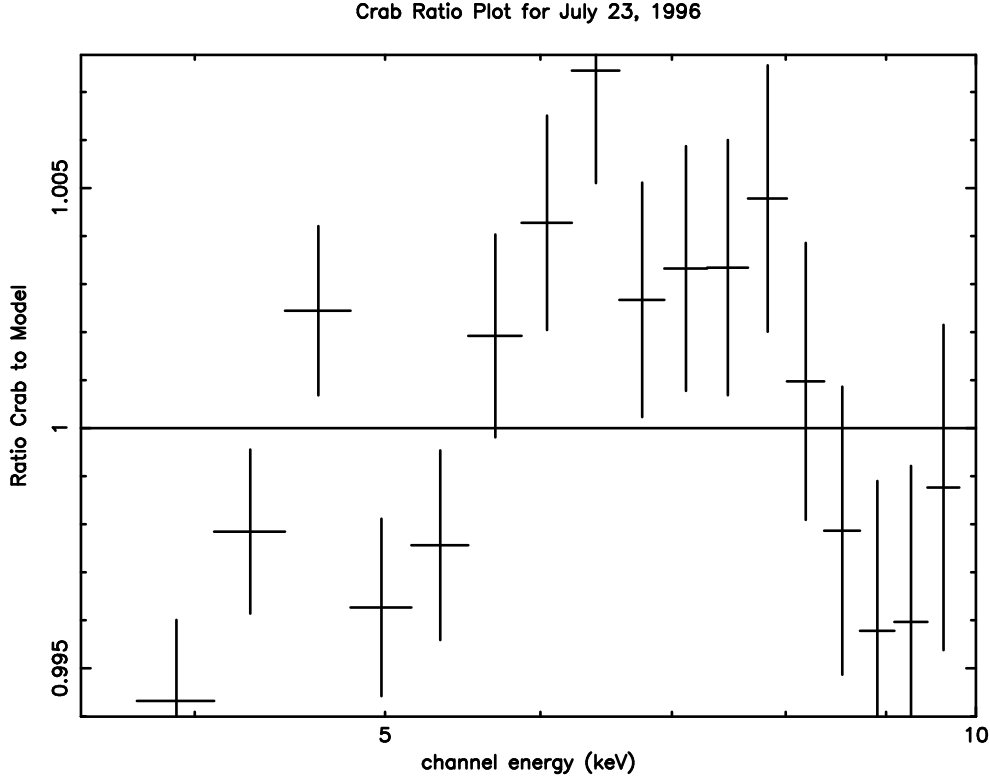


Figure 1. The ratio of the observed Crab spectrum from July 23, 1996 to the best fit with the power law index and neutral hydrogen column fixed.

There is evidence for variability of both the optical depth and the electron temperature of the corona. Since the best fit electron temperatures are typical factors of ~ 2 -3 greater than the highest photon energy used in the fit, the temperature and optical depth are somewhat degenerate parameters, and small errors in either the response matrix or the model itself could result in significant deviations from the real values of the optical depth and temperature. Furthermore, the soft state and the transition state of Cygnus X-1 have been shown to have strong non-thermal electron components (Gierlinski et al. 1999; Frontera et al. 2001),

so the physical interpretation of the optical depth and temperature derived from the best-fit thermal Comptonisation model is not clear. Thus while the observations suggest that the changes in the optical depth of the system are more important than the changes in the temperature, one can only be certain that the Compton y parameter,

$$y = (4k_B T)/(m_e c^2) \text{Max}(\tau, \tau^2)$$

has changed, and not which component has actually changed.

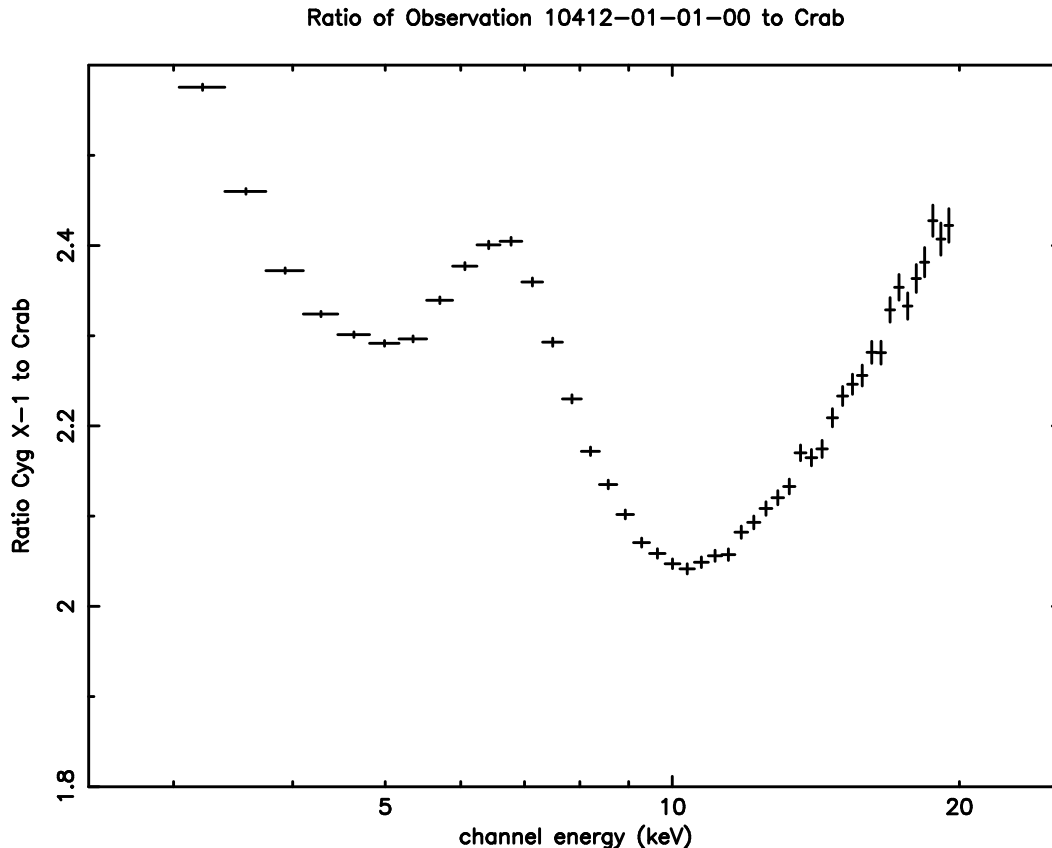


Figure 2. The ratio of observation 10412-01-01-00 to the same Crab spectrum. A strong feature is clearly seen peaking between 6 and 7 keV, so the iron line is unlikely to be a systematic feature. The plotted errors are 1σ errors.

4.2 Soft state - full integrations

In the soft state, the best fitting blackbody temperature is about 380 eV, slightly lower than the best fit for the transition state, but consistent with having the same value as in the transition state. The iron lines show a slightly greater equivalent width than in the transition state, typically around 370 eV, consistent with BeppoSax observations of the soft state (Frontera et al. 2001). The most significant difference between the fit parameters to the integrated spectra of the two states is that the optical depths are systematically lower in the soft state than in the transition state. As noted above, this can safely be interpreted only as a lowering of the Compton y parameter, i.e., a smaller typical amplification of the energy of a seed photon in the soft state than in the transition state.

4.3 Short integrations

4.3.1 Procedure

Having established an appropriate model for the long integrations, we then fit this model to the data for the 16 second segments. The standard 0.3 % systematic errors are added to each channel. The iron line energy, iron line physical width and the coronal temperature are frozen to the values from the full integrations (leaving 13 degrees of freedom), but even when allowed to vary, they typically differ by no more than $\sim 10\%$ different than the values from the full

integrations. These parameters are frozen because the fits are least sensitive to them and because the χ^2 values that are significantly below 1 for the full integrations suggest the model is “overfitting” the data. The optical depth parameter is allowed to float rather than the coronal electron temperature simply because the optical depth is observed to vary more dramatically in the best fits, and not for any physically motivated reason. The two parameters are essentially degenerate given the energy range being fit.

4.3.2 Results

The χ^2/ν values for the 16 second fits are typically about 1.0 (the mean χ^2/ν is 1.01 for the soft state and 0.94 for the transition state), and never larger than 2.8, nor smaller than 0.22. Since over 1000 fits have been done, a few outliers at relatively large and relatively small χ^2/ν are to be expected. Errors in the best fit parameters are estimated using the steppar command within XSPEC on a representative sample of the fits (direct computations of all the errors is not computationally feasible for this large number of fits). Typical 90% errors in the iron line flux level are about 20%, errors in the optical depth are 5%, and errors in the blackbody temperature are 25%.

We then look for the amplitude of variations of the different fit parameters and for correlations in their variations. In table 3, the fractional RMS variations of the fit parameters are presented. Since the 90% errors correspond to 1.65

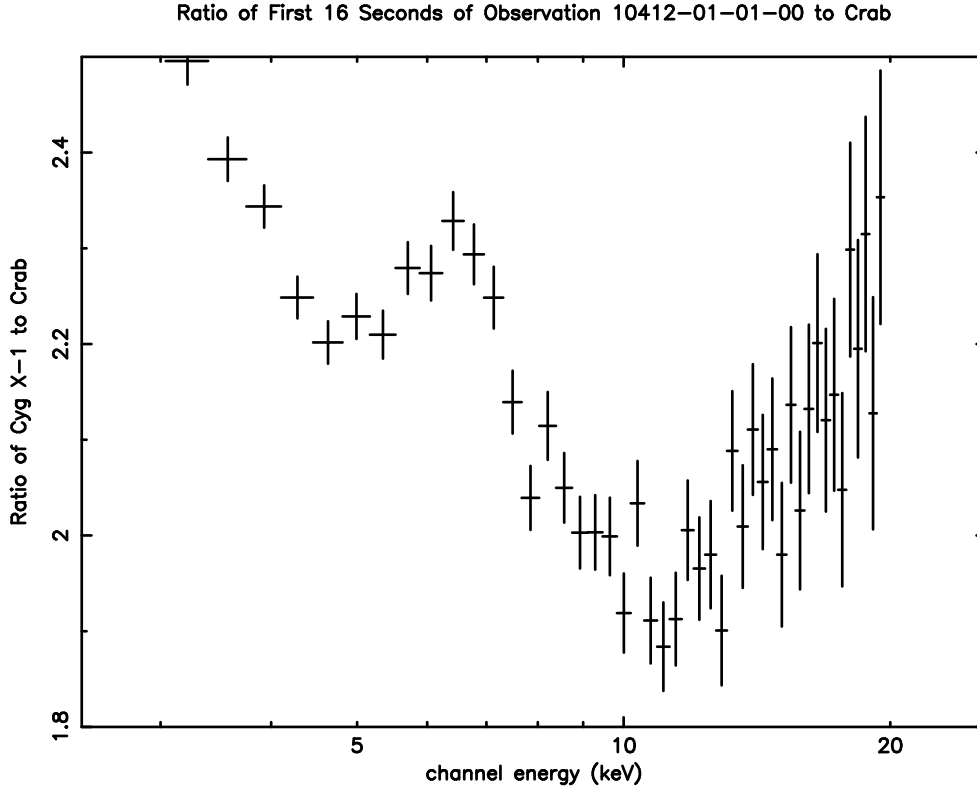


Figure 3. The ratio of the first 16 second segment of observation 10412-01-01-00 to the same Crab spectrum. Note that the shape is essentially the same as in the previous figure. The plotted errors are 1σ errors.

σ variations, the random errors expected are about 12% in iron line flux, 3% in optical depth, and 15% in blackbody temperature. One cannot explicitly fit the equivalent width in XSPEC, so one cannot derive explicit error bars, but they should be slightly larger than those of the iron line flux normalization, since there are errors in both the flux of the line and of the underlying continuum. The errors in the overall flux should be quite small ($< 1\%$).

It is thus clear that the line normalisation, the overall flux, and τ vary on 16 second timescales. The line normalisation tracks the overall flux, while the equivalent width does not. In all the observations except 10412-01-01-00, the iron line normalisation tracks very well with the best fit value of τ . A typical plot (from observation 10512-01-09-01) is shown in Figure 5.4a. Since the optical depth is a proxy for the spectral index of the power law, and the line normalization correlates with the continuum flux, what this correlation really shows is that in general, the spectrum gets harder as the source gets brighter. Why observation 10412-01-01-00 does not fit the trend is unclear. The errors for the best fit τ and $k_B T_{cor}$ to the full integration are much larger than for the other observations, so the most likely explanation is that the initial parameters for the short timescale fits are somehow in error, but a real physical difference between this observation and the others cannot be ruled out. However, the optical depth does not correlate with the equivalent width, as is shown in Figure 5.4b. The maximum variations in the flux are factors of 2.6 within individual observations (in obs 10512-01-08-00), 6 across the whole set of soft state

observations, and 3 across the whole set of transition state observations.

The blackbody temperature and the iron line equivalent width show variability that is generally consistent with or less than the fitting errors. In the cases where the variability is less than that expected due to the errors, the likely cause is that the systematic errors contribute to the size of the fitting errors, but do not contribute to the variability. We thus confirm previous results (Gilfanov, Churazov & Revnitsev 2000) that the seed photon component shows little if any intrinsic variability on relatively short timescales. Since these two components show no evidence of variability, any correlations between their values and those of other parameters would likely be due to errors in the fit parameters rather than intrinsic correlations, so we do not discuss any such possible correlations. We do plot the iron line equivalent width versus flux (3.5 to 10 keV) for observation 10412-01-01-00 in Figure 5.5. These results are typical of all the observations and demonstrate that there is no correlation between line equivalent width and overall flux. Furthermore, one can see from the plot that the variations in the equivalent width are consistent with being due to the fit errors.

5 COMPARISON TO THE HARD STATE

It has been previously shown that in the hard state of Cygnus X-1, the variability must be driven by changes in the corona's properties rather than changes in the properties of the seed photon distribution (Maccarone, Coppi, & Poutanen 2000; Böttcher 2001). One of the key pieces of ev-

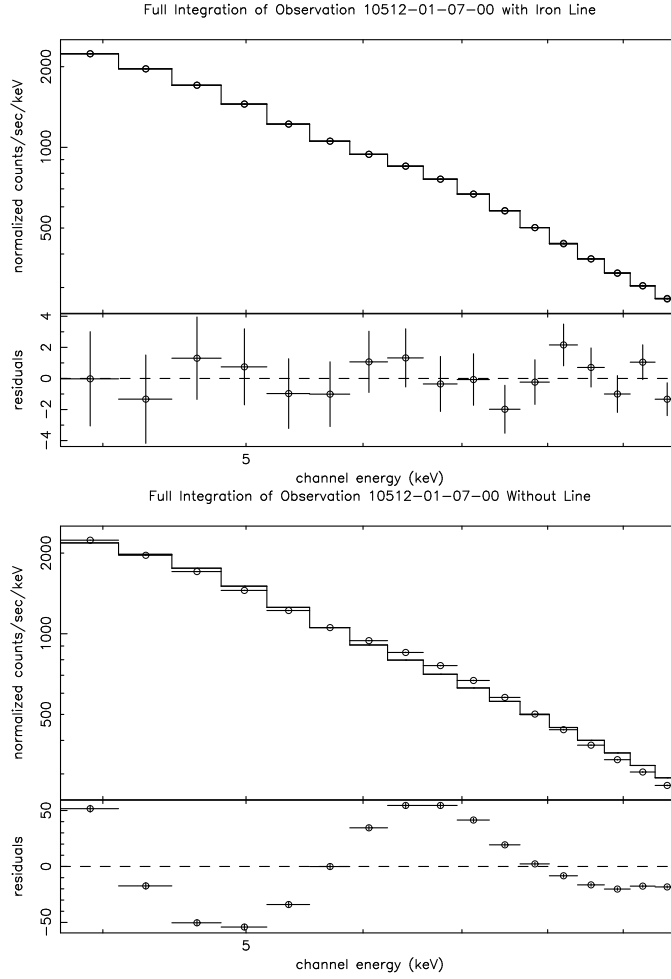


Figure 4. The full integration of Proposal 10512-01-07-00. Top: Fit and residuals with line. Bottom: Fit and residuals without line. The errors shown in the residuals represent only the statistical errors. Small circles are used in both plots to identify the actual data points, while the model is shown by the solid line. Where the error bars are not seen, they are smaller than the width of the line showing the model. The plotted errors are 1σ errors.

ObsID	T_{BB}	τ	LN	EqW	Flux
10412-01-01-00	.158	.309	.216	.124	.158
10412-01-02-00	.086	.058	.139	.126	.084
10412-01-03-00	.105	.073	.153	.145	.127
10412-01-05-00	.220	.204	.152	.110	.081
10412-01-06-00	.161	.118	.189	.173	.133
10512-01-07-00	.014	.063	.229	.110	.189
10512-01-07-02	.015	.071	.211	.175	.181
10512-01-08-01	.103	.071	.242	.120	.222
10512-01-08-02	.095	.122	.238	.163	.169
10512-01-08-00	.100	.071	.195	.141	.149
10512-01-09-00	.093	.135	.215	.148	.169
10512-01-09-01	.093	.059	.219	.128	.191
10512-01-09-02	.100	.133	.187	.167	.101

Table 3. The fractional variances of each fit parameter for the 16 second segment within the observations.

idence for this in hard state observations is that the typical shot duration decreases with increasing energy. This observation rules out light-travel time models for the time lags seen in the hard states of X-ray binaries (see e.g. Kazanas, Hua, & Titarchuk 1997). The time lag spectra in the hard and soft state have been shown to be similar to one another (Pottschmidt et al. 2000). Additionally, we have now shown

that the seed photon component is much less variable than the coronal component of the spectrum, in concordance with the results of Gilfanov et al. (2000) who found a blackbody-type spectrum in their phase resolved spectroscopy that showed up only at zero frequency. Finally we present in Figure 5.8 the autocorrelations and cross-correlations of the three spectral states and show that qualitatively, the same

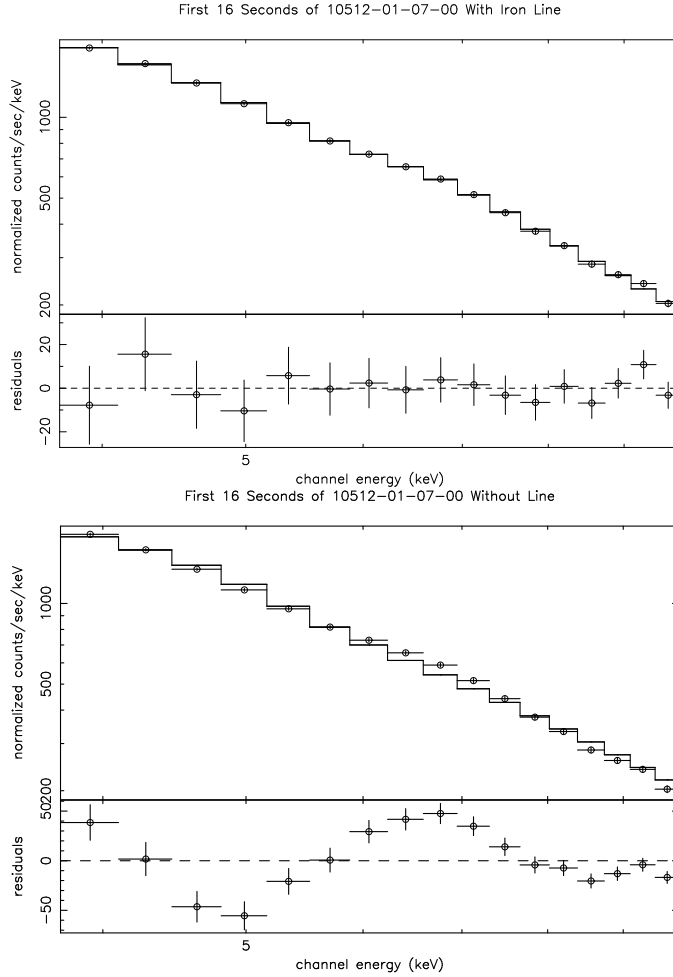


Figure 5. The fit to the first 16 seconds of Proposal 10512-01-07-00. Top: Fit and residuals with line. Bottom: Fit and residuals without line. The $\Delta\chi^2$ for the two observations is 329, so the iron line is extremely significant even on this short timescale. The actual data points are indicated by small circles, and the best fitting model is shown by the solid line. Where the error bars cannot be seen, they are smaller than the width of the line showing the model. The plotted errors are 1σ errors.

trends occur in all three. In all cases, the typical variability timescale is longer at lower energies. Since the variability is driven by changes in the corona in all cases and the qualitative trend of typical variability timescale versus energy is also the same, it seems likely that a single origin might explain the variability in all three states.

6 SUMMARY

We find that the equivalent width of the iron line in Cygnus X-1 remains constant on 16 second timescales in the soft state, despite changes in continuum flux by factors of order 3. A constant equivalent width indicates that the line intensity and the continuum intensity vary together, i.e. the phase of the line variations is the same as that of the continuum variations. This observation suggests that (1) the line flux level has now been definitively shown to correlate with the continuum flux level on short timescales, (2) at least 80% of both the line and the continuum fluxes comes from within about 16 light seconds of the black hole (most likely nearly 100% of the flux comes from these distances, but the fit errors preclude a stronger statement) and (3) it is unlikely

that major changes in the accretion geometry occur during the soft state.

We find essentially the same results for the transition state. There is suggestive evidence that the iron line equivalent width evolves over the transition state. (In fact this almost certainly must be the case since the equivalent widths in the soft state are slightly larger than those in the transition state). Thus we find again, that the line flux is correlated with the continuum flux level, that the bulk of the X-ray luminosity in both the line and in the continuum must come from within 16 light-seconds, and that there are unlikely to be major geometry changes in the accretion flow in the transition state on short timescales (i.e. less than 10000 seconds).

It is worth noting that the requirement that essentially all the iron line flux comes from within 16 light seconds requires that the emission comes from reflection off the accretion disc, and not off the companion star or the outer portion of the stellar wind that makes the accretion stream, since for the 5.6 day orbit and roughly $30 M_{\odot}$ total mass of the Cyg X-1/HD 226868 system, the binary separation between the black hole and its companion star is roughly 0.2

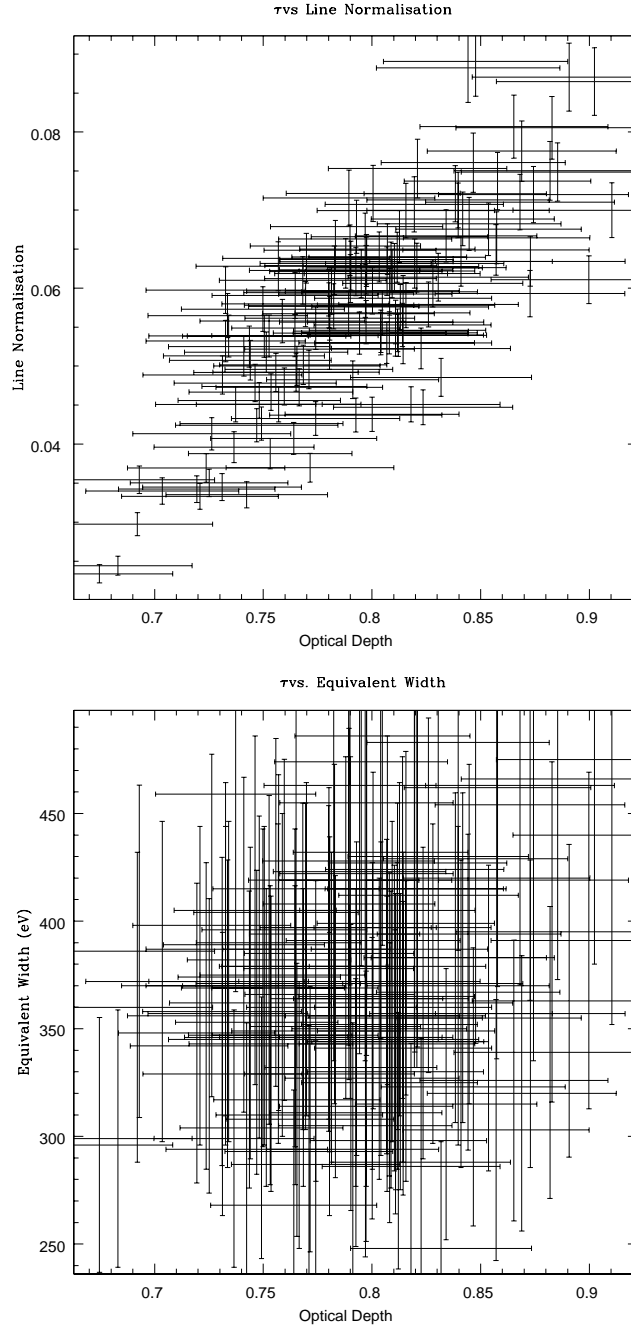


Figure 6. (a) The correlation between optical depth and the line normalisation. (b) The lack of a correlation between optical depth and the line equivalent width. The figures are plotted from observation 10512-01-09-01, the longest soft state observation. The plotted errors show the 90% confidence intervals.

AU, or 100 light-seconds. Since this is substantially larger than the 16 light-seconds on which we observe the changes in the line and continuum intensities, one would expect to observe an anti-correlation between equivalent width and continuum intensity as well as a time delay between continuum rises and line intensity rises if a substantial portion of the line emission was due to reflection off the companion star. This finding is in accord with the observation from ASCA that, in the hard state, the iron line equivalent width can drop to less than 30 eV in the hard state (e.g. Ebisawa et

al. 1996), which provides an upper limit for the reprocessing effects of the companion star and its wind.

Our two key results, (1) that no variability is detected in the seed photon component on timescales where the hard component varies strongly and (2) that the iron line flux variations track the continuum flux variations, supply strong constraints on the nature of the processes driving the X-ray variability. One might expect to see changes in the properties of the blackbody as a result of the energy deposited in the disc by the Compton reflection process. However, the

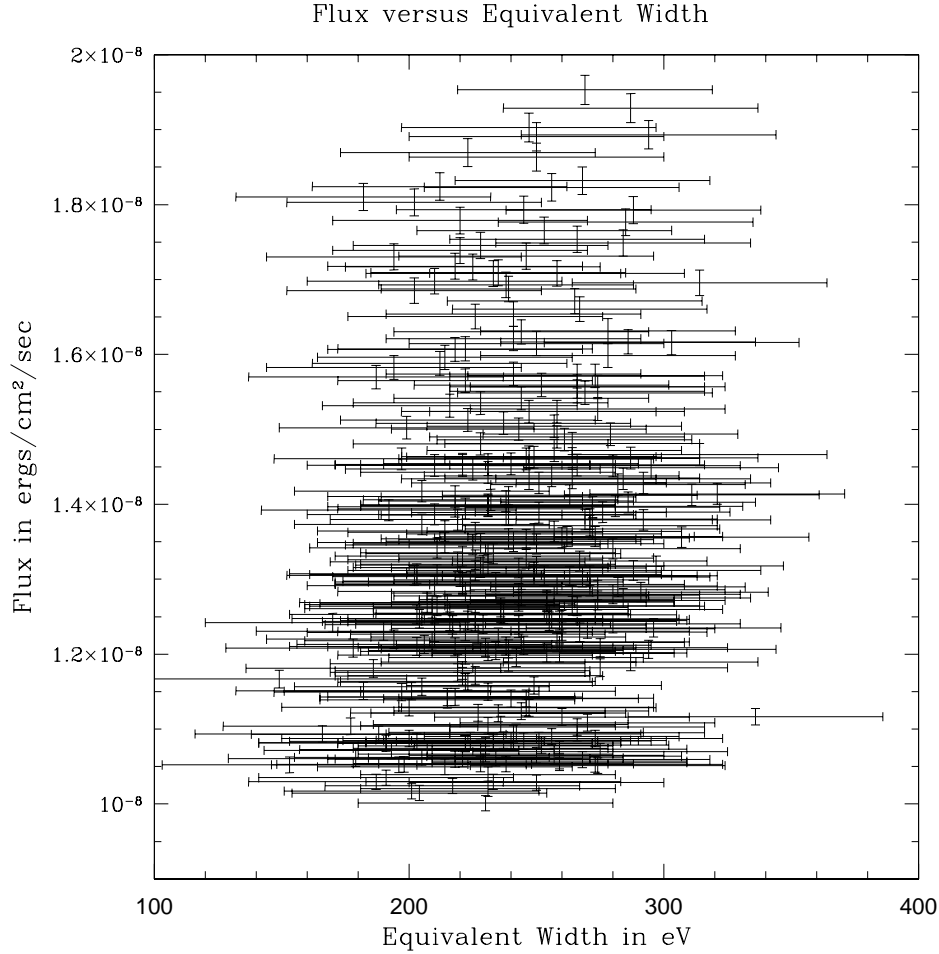


Figure 7. The plot of flux versus equivalent width of the iron line for observation 10412-01-01-00. It is clear that the variations between the two parameters have no correlation and that the variations in the iron line equivalent width are consistent with the random errors. The plotted errors show the 90% confidence intervals.

corona's contribution to the total energetics of the system in the soft and transition states is typically of order 20%, so the soft component dominates the overall energetics of the system (Frontera et al. 2001). Moreover, since the short timescale variability of the coronal luminosity is only about 10%, the seed photon component would be expected to vary by only a few percent even if Compton reflection deposited 100% of the hard photons' energy into the disc. Thus, assuming the disc is intrinsically steady, one should not be too surprised to see no evidence for the disc varying, assuming that the disc is intrinsically steady. Both the steadiness of the disc component and the correlation between y and the line strength suggest that the variability is instead driven by changes in the properties of the corona, e.g., as in the spectral evolution model of Poutanen & Fabian 1999, rather than by changes in the soft photon flux with a steady corona present (see e.g. Kazanas, Hua & Titarchuk 1997; Böttcher & Liang 1999). The models of spectral variability in accreting black holes have been developed almost entirely with the hard state in mind, but the observations of Cygnus X-1 in the soft and transition states are qualitatively consistent with what is seen in the hard state of Cygnus X-1 in that coronal variations rather than modulation of the soft compo-

nent must be invoked (see e.g. Maccarone, Coppi, & Poutanen 2000). Furthermore, our finding that the disc appears intrinsically steady is in good agreement with observations of other systems where the soft state spectra show essentially no power law tails and the soft state lightcurves show essentially no variability.

7 ACKNOWLEDGEMENTS

We wish to thank Mike Nowak and Raj Jain for useful discussions. We thank Charles Bailyn and Cole Miller for critical readings of this manuscript and hope the readers of this work are grateful for their insistence that the plots be made such that the data and model could be distinguished more easily. We are indebted to the anonymous referee for numerous suggestions that improved the quality of this work substantially. This work has made use of data obtained from the HEASARC online archive operated by NASA's Goddard Space Flight Center.

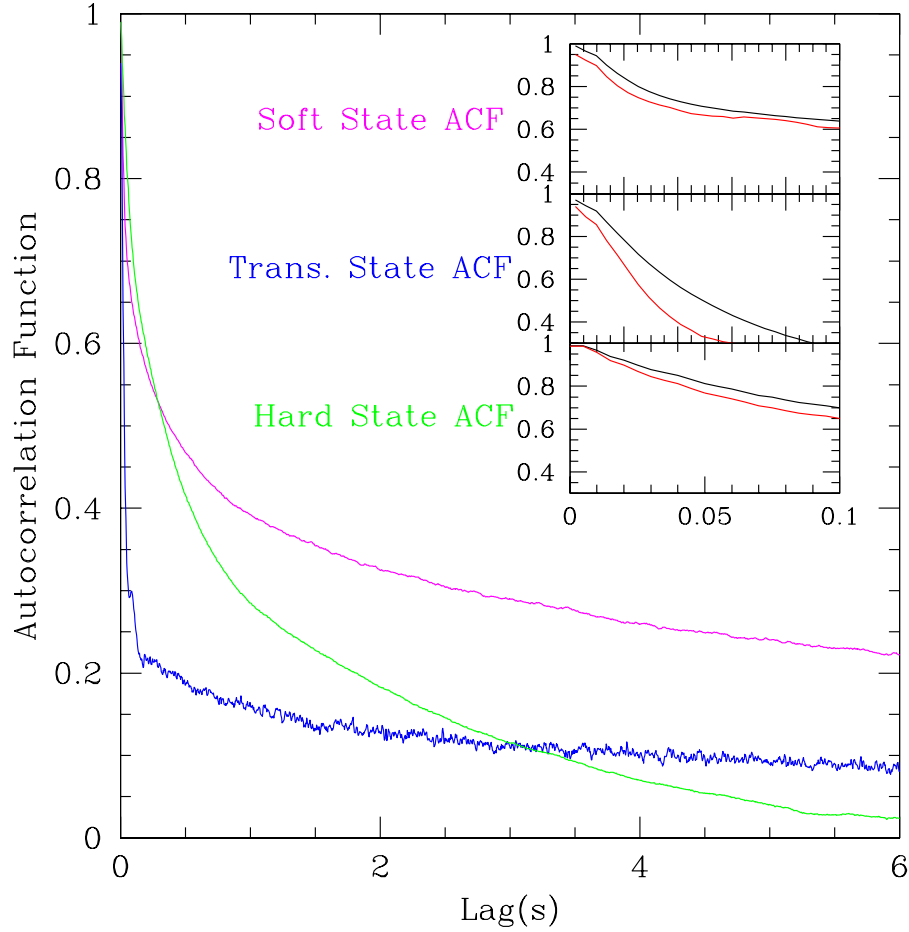


Figure 8. The autocorrelations in the three spectral states. For the large graph, the soft state is in purple, the transition state in blue and the hard state in green. For the inset boxes, the 2-5 keV ACF is in black while the 5-13 keV ACF is in red.

REFERENCES

- Antonucci, R.R.J. & Miller, J.S., 1985, *ApJ*, 297, 621
 Arnaud, K.A., 1996, in *Astronomical Data Analysis Software and Systems V*, ASP, Conf. Ser., Vol. 101, Jacoby, G., & Barnes, J., eds., (ASP: San Francisco), p. 17
 Basko, M., Sunyaev, R., & Titarchuk, L., 1974, *A&A*, 31, 249
 Böttcher, M., 2001, *ApJ*, 550, 963
 Böttcher, M. & Liang, E.P., 1999, *ApJL*, 511, L37
 Bradt, H.V., Rothschild, R.E., & Swank, J.H., 1993, *A&AS*, 97, 355
 Ebisawa, K., Ueda, Y., Inoue, H., Tanaka, Y., & White, N.E., 1996, *ApJ*, 467, 419
 Frontera, F. et al. 2001, *ApJ*, 546, 1027
 George, I.M., & Fabian, A.C., 1991, *MNRAS*, 249, 352
 Gierlinski, M., Zdziarski, A.A., Poutanen, J., Coppi, P.S., Ebisawa, K., & Johnson, W.N., 1999, *MNRAS*, 309, 496
 Gilfanov, M., Churazov, E., & Revnivtsev, M., 2000, *MNRAS*, 316, 923
 Kazanas, D., Hua, X.-M., & Titarchuk, L., 1997, *ApJ*, 480, 735
 Lee, J.C., Fabian, A.C., Reynolds, C.S., Brandt, W.N., & Iwasawa, K., 2000, *MNRAS*, 318, 857
 Maccarone, T.J., Coppi, P.S., & Poutanen, J., 2000, *ApJL*, 537, L107
 Magdziarz, P. & Zdziarski, A.A., 1995, *MNRAS*, 273, 837
 Mitsuda, K., Inoue, H., Koyama, K., Makishima, K., Matsuoka, M., Ogawara, Y., Suzuki, K., Tanaka, Y., Shibasaki, N., Hirano, T., 1984, *PASJ*, 36, 741
 Nandra, K., George, I.M., Mushotzky, R.F., Turner, T.J., & Yaqoob, T., 1999, *ApJL*, 523, L17
 Nishimura, J., Mitsuda, K., & Itoh, M., 1986, *PASJ*, 38, 819
 Nowak, M.A., 1995, *PASP*, 107, 1207
 Pottschmidt, K., Wilms, J., Nowak, M.A., Heindl, W.A., Smith, D.M., & Staubert, R., 2000, *A&A*, 357, 17L
 Poutanen, J., & Fabian, A.C., 1999, *MNRAS*, 306, L31
 Shakura, N., & Sunyaev, R., 1973, *A&A*, 24, 337
 Wang, J.X., Zhou, Y.Y., Xu, H.G., & Wang, T.G., 1999, *ApJ*, 516, L65
 Weaver, K.A. & Reynolds, C., 1998, *ApJL*, 503, L39
 Yaqoob, T., Serlemitsos, P.J., Turner, T.J., George, I.M., & Nandra, K., 1999, *ApJL*, 470, L27